JACS
JOURNAL OF THE AMERICAN CHEMICAL SOCIETY
pubs.acs.org/JACS

Article

A Spin Frustrated Hourglass {Gd_9} Molecular Nanomagnet with Unusual Magnetocaloric Properties

Sai P. K. Panguluri, Eufemio Moreno-Pineda,* Concepción Molina-Jirón, Sagar Paul, Marc Ubach I Cervera, Emmanouil K. Charkiolakis, David Gracia, Marco Affronte, Wolfgang Wernsdorfer, Marco Evangelisti,* Jürgen Schnack,* and Mario Ruben*

Cite This: https://doi.org/10.1021/jacs.5c13048

Read Online

ACCESS | Metrics & More | Article Recommendations | Supporting Information

ABSTRACT: We report a highly symmetric {Gd_9} molecular nanocage with the formula $[Gd_9(BA)_{16}(OH)_{10}]Cl{\cdot}3(C_2H_5OH){\cdot}4(H_2O)$, which crystallizes in the cubic space group $Pn\bar{3}n$. The structure features two crystallographically distinct Gd^{3+} ions, forming highly regular triangular Gd^{3+} arrangements leading to a geometrically frustrated magnetic network. Magnetization measurements at 2 K reveal a broad plateau between 1.5 and 4 T, while zero-field heat capacity shows a Schottky anomaly centered at 0.6 K—indicative of low-lying excited states and competing magnetic interactions. The magnetocaloric effect, evaluated through both direct and indirect methods, exhibits a re-entrant profile in the isentropic curves, pointing to a nontrivial evolution of magnetic entropy under applied fields. To probe the origin of this behavior, we employed the finite-temperature Lanczos method on a model spin Hamiltonian. The results reveal that the antiferromagnetic exchange between Gd^{3+} ions, combined with the frustration inherent to the {Gd_9} geometry, leads to a degenerate ground state. An external field lifts this degeneracy, producing a regime with a sharply reduced density of states between 1.5 and 4 K, which underlies the unconventional magnetocaloric response. The {Gd_9} cage thus represents a rare example of a spin-frustrated arrangement arising from competing antiferromagnetic interactions between the Gd^{3+}. These findings demonstrate how frustrated topologies and tunable low-energy excitations can be exploited to modulate the magnetothermal properties, with potential implications for cryogenic magnetic cooling technologies.

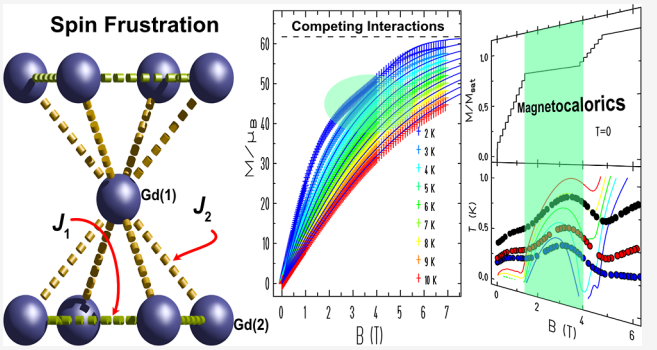

INTRODUCTION

In magnetic systems, the impossibility of simultaneously satisfying pairwise interactions gives rise to frustration, typically due to geometric or exchange constraints.[1,2] Geometric spin frustration—where the topology of the lattice alone prevents the full minimization of exchange energies—suppresses classical magnetic order and stabilizes a range of unconventional ground states.[1] This phenomenon is especially pronounced in triangular lattices,[3−5] where antiferromagnetic coupling among half-integer spins in odd-membered rings creates a macroscopically degenerate manifold.

Crucially, such behavior is not confined to extended lattices: zero-dimensional molecular architectures, particularly coordination compounds, frequently incorporate triangular spin motifs.[6−9] These discrete systems offer synthetically tunable platforms for probing frustration at the molecular scale.[10] Frustrated molecular nanomagnets (FMN) are increasingly recognized as promising candidates for magnetocaloric applications. Their discrete energy spectra, well-defined spin states, and chemical modularity allow fine control over magnetic entropy.[11−13] Moreover, spin frustration enhances the magnetocaloric effect (MCE) at low temperatures by broadening the temperature range of paramagnetic-like behavior. Besides, it increases the density of low-lying spin states and enables field-tunable degeneracies, resulting in large isothermal entropy changes and pronounced adiabatic temperature shifts under applied magnetic fields—key performance metrics in solid-state refrigeration.[6]

The investigation of molecular nanomagnets for subkelvin magneto refrigeration typically relies on isotropic ions with large magnetic moments,[8,12−17] although anisotropic systems[18,19] can likewise be considered. However, unlike paramagnetic salts, FMN exhibits complex magnetothermal behavior arising from internal exchange interactions and quantum level crossings.[2] These phenomena, associated with

Received: July 30, 2025
Revised: October 1, 2025
Accepted: October 2, 2025

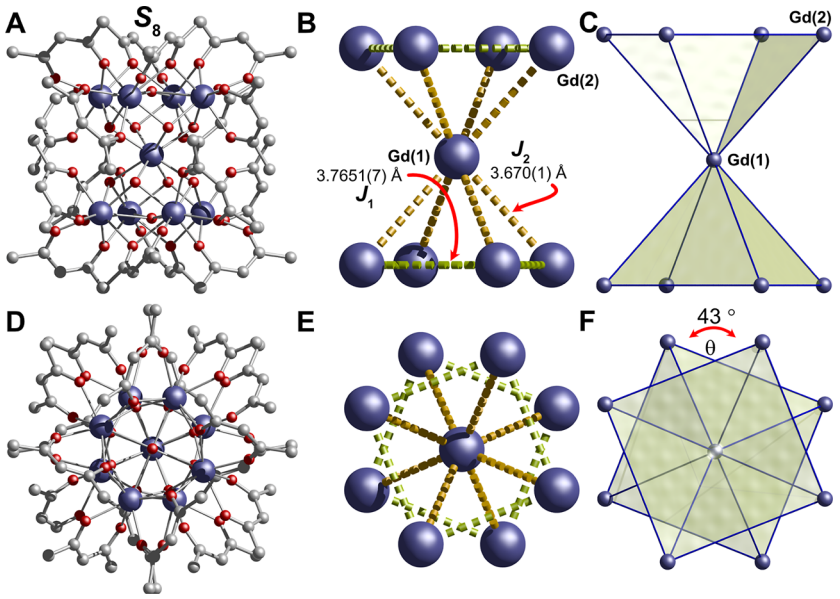

Figure 1. Crystal structure of $[Gd_9(BA)_{16}OH_{10}]Cl$ {**Gd_9**} side (A−C) and top view (D−F), highlighting the highly regular structure with triangular Gd^{3+} arrangements. The yellow and green dotted lines in panels (B,E) depict the two different interactions occurring in the {**Gd_9**} cage. Color code: Gd, blue; O, red; C, gray. Hydrogens omitted for clarity.

quantum phase transitions, enable sharp entropy redistributions that amplify the MCE. Additionally, frustration preserves residual entropy at zero temperature, enabling rapid cooling near the saturation field.[20−22] On the quest for further understanding of frustration effects on FMN, here, we investigate a highly symmetric molecular cage, with formula $[Gd_9(BA)_{16}(OH)_{10}]Cl{\cdot}3(C_2H_5OH){\cdot}4(H_2O)$ (where BA = benzoylacetonate ({**Gd_9**})) with an hourglass-like molecular structure (Figure 1). The complex, featuring four {**Gd_3**} vertex-sharing triangular Gd^{3+} motifs, displays frustration of its energy manifold; hence, it exhibits a strongly field-dependent density of states and a tunable magnetocaloric response, highlighting the importance of the energy landscape engineering for molecular coolants.

RESULTS AND DISCUSSION

The hourglass-like complex crystallizes in the $Pn\bar{3}n$ space group, with six cationic {**Gd_9**} cages residing per unit cell. Three differently oriented molecules compose the unit cell, with the shortest Gd···Gd distance being 12.904 Å (See Figure S1). The asymmetric unit represents one-eighth of the molecule, indicating that the complete cage exhibits S_8 symmetry. The {**Gd_9**} cage consists of two pentanuclear square pyramids sharing a central Gd^{3+} ion, forming an hourglass-like shape (Figure 1C,D). These pyramids are twisted relative to each other by about 45°, resulting in a square antiprismatic geometry at the central Gd^{3+} ion (Figure 1B).

Single-crystal X-ray diffraction reveals that the cage contains only two distinct types of Gd^{3+} ions: the central ion (Gd(1)) is octacoordinated, possessing a nearly perfect square antiprismatic geometry with D_{4d} symmetry, as confirmed by Continuous Shape Measures[23] (CShM, Table S1). Its coordination sphere consists exclusively of eight μ_3-OH^- groups; the eight peripheral ions (Gd(2)), also octacoordinated, but with a more irregular geometry. Each Gd^{3+} ion is chelated by three BA^- ligands—two with coordination mode μ-BA(κ^2O,O′; κ^1O) and one with μ-BA(κ^2O,O′)—along with two μ_3-OH^- groups. These ions adopt a trigonal dodecahedral geometry with D_{2d} symmetry (Table S1).

The metallic core of the {**Gd_9**} cage can also be described as a pyramidal assembly of four {**Gd_3**} triangles, each formed by one Gd(1) and two Gd(2) ions. These triangles share Gd(1) as a common vertex, while also sharing edges with adjacent triangles. Each Gd(2) is stabilized by a μ_3-OH^- bridge and is collectively capped by a μ_4-OH^- group at the base of the pyramid. The Bond Valence Sum (BVS) for the μ_3-OH^- is found to be 1.073, while for the μ_4-OH^-, the BVS is 1.02, both being consistent with OH^- groups.[24] The overall complex is charge-balanced by a Cl^- ion. Due to the highly symmetric triangular arrangement of Gd^{3+} ions within the {**Gd_9**} cage, magnetic frustration effects are likely to occur.

To explore how the highly regular {**Gd_9**} cage influences the magnetic behavior, we conducted magnetic susceptibility ($\chi_M \equiv M/B$) measurements. The χ_M properties were collected employing a polycrystalline sample under an applied field of 0.1 T in the temperature range of 2−300 K (top panel in Figure 2). At room temperature, the $\chi_M T$ value amounts to 67.4 emu K mol^{-1}, in line with nine $^8S_{7/2}$ ions (cf. 68 emu K mol^{-1} for nine noninteracting $s = 7/2$ ions with $g = 1.96$). As the temperature decreases, the $\chi_M T(T)$ remains nearly constant down to ca. 20 K, where it sharply drops to 29.3 emu K mol^{-1}. The downturn is indicative of antiferromagnetic interactions within the cage, as commonly observed in systems with similarly highly symmetric motifs.

Magnetization studies (M) were conducted in the temperature range of 2−10 K and with applied fields between 0 and 7 T. The $M(B,T)$ data shows that saturation is achieved for fields above 6 T (bottom panel in Figure 2). Remarkably, a plateau is also observed between 1.5 and 4 T for the $M(B)$ traces below 3 K. Note that such a type of plateau is uncommon in lanthanide-based complexes and is a signature of spin frustration effects.[2] To further investigate the system, we employed μSQUID arrays from 5 K down to 30 mK, in the field range of ±1.4 T. No major structure is revealed in the $M(B)$ loops. Notably, the $M(B)$ loops above 2 K, however,

https://doi.org/10.1021/jacs.5c13048
J. Am. Chem. Soc. XXXX, XXX, XXX−XXX

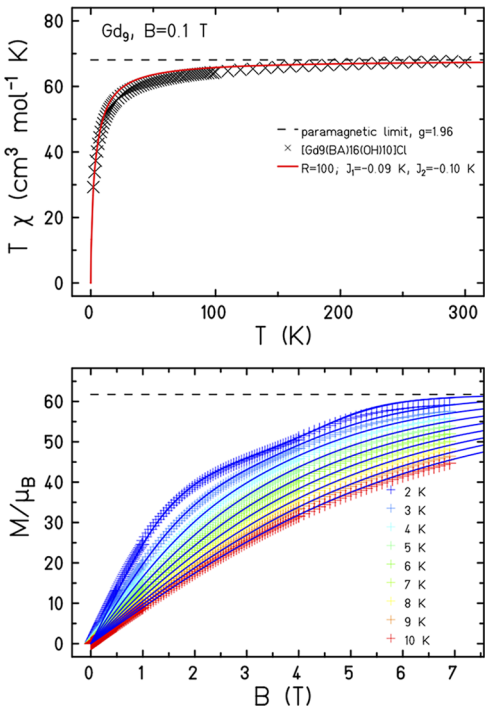

Figure 2. Magnetic susceptibility versus temperature ($\chi_M T$, T) at B = 0.1 T (top) and magnetization versus applied magnetic field (M, B) for temperatures from 10 down to 2 K (bottom). R is the number of random vectors employed for the computation. The experimental data are given by symbols, while the theoretical calculations are shown by curves (see text).

yield a vanishing magnetic signal, likely due to the large density of populated states at such temperature and field, a signature of frustration (See Figure S3).

A better insight into the magnetic characteristics of {$\mathbf{Gd_9}$} can be gained by conducting field-dependent heat capacity (c_p) studies. These studies are a powerful tool for probing spin frustration in molecular nanomagnets, since they sensitively capture low-energy excitations and quantum level crossings, offering insight into the system's magnetic energy landscape.[5−7,17] The c_p response of {$\mathbf{Gd_9}$} under different magnetic fields was investigated between 30 K and 50 mK with fields up to 7 T (Figure 3).

In the temperature range above liquid helium, c_p is predominantly influenced by the nonmagnetic lattice contribution, which can be effectively represented by the Debye function. This analysis leads to the determination of the characteristic Debye temperature, θ_D, calculated to be 27.7 K. Interestingly, the zero-field data exhibit no lambda-like anomaly, indicating the absence of any phase transitions. Instead, the data are marked by a broad Schottky-like anomaly centered around 0.6 K. This anomaly not only shifts to higher temperatures but also increases in magnitude with the application of a magnetic field. Below the temperature range of 60−70 mK, the zero-field c_p appears to plateau.

The entropy at constant magnetic field, $S = \int c_p/T dT$ (Figure S4), was used to obtain the MCE main figure of merit, namely the magnetic entropy change ($-\Delta S_m$, Figure S5). The $-\Delta S_m$ reaches a maximal 23.1 J kg^{-1} K^{-1} at temperature T = 2.1 K and magnetic field change ΔB = 7 T, which corresponds to 79% of the available entropy, i.e., R ln (2s + 1) = 29.1 J kg^{-1} K^{-1}. Besides indirect estimations, the MCE was also measured directly (Figure 4, bottom panel, and Supporting Information for details). We conducted demagnetization processes starting from a relatively high magnetic field of B = 8 T, while varying the initial temperatures T_0. As a representative example, when T_0 is set to 1.0 K, we observed that the sample temperature initially decreases linearly as the magnetic field B decreases,

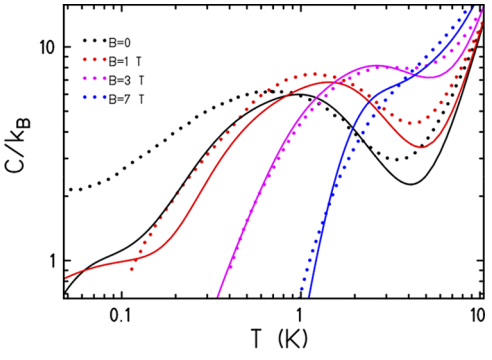

Figure 3. Heat capacity (c_p) per molecule as a function of temperature T for various magnetic fields B. The dots denote experimental values, while the curves are theoretical calculations.

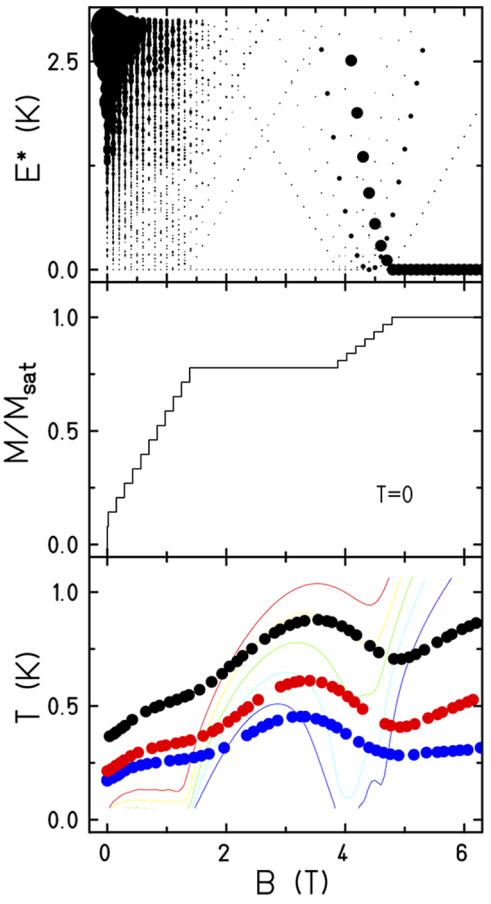

Figure 4. (top panel) Zeeman diagram of low-lying energy levels; the size of the bullet points reflects the weight of the respective energy in the FTLM. $E^* = E_i - E_0$, where E_i and E_0 are the energies of the ith and ground Zeeman states, respectively, at the respective field. (middle panel) Normalized magnetization $M(B)$ curve at zero temperature. (bottom panel) Calculated (thin curves) and directly measured (symbols) isentropes, i.e., curves of constant entropy.

https://doi.org/10.1021/jacs.5c13048
J. Am. Chem. Soc. XXXX, XXX, XXX−XXX

which aligns with the expected behavior of a paramagnet. Notably, between the magnetic field values of B = 4.8 and 1.5 T, a bump anomaly is encountered in the temperature readings. Specifically, the temperature first experiences an increase as B decreases to 3.4 T, demonstrating an inverse MCE. Following this, the temperature steadily declines with further decreases in B down to 1.5 T. Below B = 1.5 T, there is a smaller, yet discernible bump anomaly centered at B = 0.6 T. Ultimately, upon completing the demagnetization process, the sample temperature stabilizes at T = 0.35 K. The inverse MCE observation is characteristic of frustrated topologies.[6,7] Note that the recorded temperatures are not adiabatic temperatures; hence, they do not fully reflect the potential of the system under ideal conditions. These readings are influenced not only by the magnetothermal properties of {Gd_9} but also by the unique characteristics of the sample and experimental setup used. Due to the inevitable heat exchanged between the sample and the thermal bath, lower temperatures should be achieved under adiabatic conditions.

To comprehend the overall magnetic behavior of {Gd_9}, the magnetic and magnetothermal data were modeled with the Hamiltonian of the form (1)

$$\hat{H} = -2J_1 \sum_{i<j(squares)} \hat{\vec{s}}_i \cdot \hat{\vec{s}}_j - 2J_2 \sum_{i=1}^{8} \hat{\vec{s}}_i \cdot \hat{\vec{s}}_9 + g\mu_B B \sum_{i=1}^{9} \hat{s}_i^z \quad (1)$$

where the first term denotes the Heisenberg exchange between neighboring spins in the two squares, the second term the exchange of all spins in squares with the central spin, and the third (Zeeman) term the interaction with the external field (See Figure 1E). In our simulations, the single-ion anisotropy is neglected, while a common g-factor of 1.96 is assumed. Since the total Hilbert space has a dimension of 134,217,728, exact diagonalization of the Hamiltonian matrix is prohibitable impossible (even when using symmetry arguments); therefore, the finite-temperature Lanczos method (FTLM) is suited as an accurate approximation.[25] For the calculation, R = 100 random vectors were used to average observables.[26] Figure 2 displays the M as $\chi_M T(T)$ at a small field (top) and $M(B)$ for various temperatures (bottom). The experimental data were used to determine the best values of J_1, J_2, and g describing both profiles. The best simulations yield J_1 = −0.09 K, J_2 = −0.10 K, and g = 1.96 (See Figures 2 and S6). We estimate that the uncertainty is not bigger than 10% of these values. With this set of parameters, we calculate the magnetic contribution to c_p, as well as the isentropes of the direct MCE measurements. The experimental c_p and simulations, together with the lattice contribution, are represented in Figure 3 as solid lines, while the simulated isentropes for ideal adiabatic conditions are depicted in Figure 4, together with the experimental data, and in Figure S7 for several entropy values. The simulations, although they do not perfectly replicate the experimental data at the lowest temperatures, offer a remarkably close description.

By understanding the energy manifold of the {Gd_9} system, we can interpret the structure of its magnetic and magnetothermal data. Figure 4 illustrates the system's unusual magnetocaloric behavior by showing how the low-lying density of states varies with the applied external magnetic field. In this context, the Zeeman energy is represented as the excitation energy above the respective ground state for each magnetic field strength. At zero field (B = 0), there is a region with a high density of states. This is followed by a range between approximately 1.5 and 4.0 T, where the density of states is significantly lower, corresponding to a broad magnetization plateau. Beyond 4.0 T, another region of high density of states appears, which then transitions into a final region of very low density, starting at the saturation field around 4.8 T. Since entropy is related to the number of thermally accessible energy levels, regions with low density of states require higher temperatures to achieve the same level of thermal occupation as regions with higher density. This variation in thermal accessibility explains the undulating shape of the isentropes shown in the lower part of Figure 4.

CONCLUSIONS

This study presents a comprehensive investigation of the {Gd_9} molecular cage, revealing its potential as a model system for exploring spin frustration and magnetocaloric effects in lanthanide-based nanomagnets. The unique double-pyramidal geometry, featuring two distinct Gd^{3+} environments and a highly symmetric arrangement, leads to antiferromagnetic interactions and geometric frustration. These features manifest in the magnetic susceptibility, magnetization, and heat capacity data, with the latter showing broad Schottky anomalies and no signs of long-range magnetic ordering. The magnetocaloric properties are particularly noteworthy: both indirect and direct measurements reveal significant entropy and temperature changes, including inverse MCE behavior—a hallmark of frustrated spin networks. Theoretical modeling using the finite-temperature Lanczos method successfully captures the essential features of the experimental data, validating the proposed exchange interactions and highlighting the role of low-lying energy states in modulating the MCE. The field-dependent density of states, with alternating regions of high and low state density, explains the observed isentropic behavior and underscores the importance of energy landscape engineering in molecular coolants. Overall, the {Gd_9} system exemplifies how molecular design can be leveraged to achieve tunable quantum thermodynamic responses, making it a promising platform for future studies in quantum magnetism and subkelvin refrigeration technologies.

ASSOCIATED CONTENT

Supporting Information

The Supporting Information is available free of charge at https://pubs.acs.org/doi/10.1021/jacs.5c13048.

Synthetic details, experimental methods, tables and supporting figures are provided (PDF)

AUTHOR INFORMATION

Corresponding Authors

Eufemio Moreno-Pineda − *Physikalisches Institut, Karlsruhe Institute of Technology, D-76131 Karlsruhe, Germany; Facultad de Ciencias Naturales, Exactas y Tecnología, Depto. de Química-Física, Universidad de Panamá, 0824 Panamá, Panamá; Facultad de Ciencias Naturales, Exactas y Tecnología, Grupo de Investigación de Materiales, Universidad de Panamá, 0824 Panamá, Panamá;* orcid.org/0000-0002-9643-0341; Email: eufemio.moreno@up.ac.pa

Marco Evangelisti − *Instituto de Nanociencia y Materiales de Aragón (INMA), CSIC & Universidad de Zaragoza, 50009*

https://doi.org/10.1021/jacs.5c13048
J. Am. Chem. Soc. XXXX, XXX, XXX−XXX

Zaragoza, Spain; orcid.org/0000-0002-8028-9064; Email: evange@unizar.es

Jürgen Schnack − *Faculty of Physics, Bielefeld University, D-33615 Bielefeld, Germany*; Email: jschnack@uni-bielefeld.de

Mario Ruben − *Institute of Quantum Materials and Technologies (IQMT), Karlsruhe Institute of Technology (KIT), 76344 Eggenstein-Leopoldshafen, Germany; Institute of Nanotechnology (INT), Karlsruhe Institute of Technology (KIT), D-76131 Karlsruhe, Germany; Centre Européen de Sciences Quantiques (CESQ), Institut de Science et d'Ingénierie Supramoléculaires (ISIS), 67083 Strasbourg Cedex, France*; orcid.org/0000-0002-7718-7016; Email: mario.ruben@kit.edu

Authors

Sai P. K. Panguluri − *Institute of Quantum Materials and Technologies (IQMT), Karlsruhe Institute of Technology (KIT), 76344 Eggenstein-Leopoldshafen, Germany*

Concepción Molina-Jirón − *Institute of Quantum Materials and Technologies (IQMT), Karlsruhe Institute of Technology (KIT), 76344 Eggenstein-Leopoldshafen, Germany; Facultad de Ciencias Naturales, Exactas y Tecnología, Grupo de Investigación de Materiales and Facultad de Ciencias Naturales, Exactas y Tecnología, Depto. de Bioquímica, Universidad de Panamá, 0824 Panamá, Panamá*

Sagar Paul − *Physikalisches Institut, Karlsruhe Institute of Technology, D-76131 Karlsruhe, Germany*; orcid.org/0000-0001-8317-5778

Marc Ubach I Cervera − *Instituto de Nanociencia y Materiales de Aragón (INMA), CSIC & Universidad de Zaragoza, 50009 Zaragoza, Spain*

Emmanouil K. Charkiolakis − *Instituto de Nanociencia y Materiales de Aragón (INMA), CSIC & Universidad de Zaragoza, 50009 Zaragoza, Spain*

David Gracia − *Instituto de Nanociencia y Materiales de Aragón (INMA), CSIC & Universidad de Zaragoza, 50009 Zaragoza, Spain*; orcid.org/0000-0002-3511-3510

Marco Affronte − *Dipartimento di Scienze Fisiche, Informatiche e Matematiche, Universita di Modena e Reggio Emilia, 41125 Modena, Italy; Istituto Nanoscienze, CNR, 41125 Modena, Italy*

Wolfgang Wernsdorfer − *Institute of Quantum Materials and Technologies (IQMT), Karlsruhe Institute of Technology (KIT), 76344 Eggenstein-Leopoldshafen, Germany; Physikalisches Institut, Karlsruhe Institute of Technology, D-76131 Karlsruhe, Germany*; orcid.org/0000-0003-4602-5257

Complete contact information is available at: https://pubs.acs.org/10.1021/jacs.5c13048

Funding

This work has received support from the EU (MSCA-DN MolCal, 101119865), MICIU/AEI/10.13039/501100011033/ and ERDF/EU (PID2021-124734OB-C21, CEX2023-001286-S), Gobierno de Aragón (E11-23R, E12-23R). E.M.-P. thanks the Alexander von Humboldt Fellowship for experienced researchers for support. W.W. thanks the German Research Foundation (DFG) for the Gottfried Wilhelm Leibniz-Award, ZVN-2020_WE 4458-5. S.P.K.P thanks the European Unions's Framework Program for Research and Innovation, Horizon 2020, under the Marie Sklodowska-Curie Grant Agreement No. 847471 (QUSTEC) for funding.

Notes

The authors declare no competing financial interest.

■ ACKNOWLEDGMENTS

We acknowledge the DFG-CCR 1573 "4f for future" (project B4) and the Karlsruhe Nano Micro Facility (KNMF, www.kit.edu/knmf) for the provision of access to instruments at their laboratories. We also thank late Dr. Andreas Eichhoefer, Dr. Christopher E. Anson, Dr. Asato Mitzuno, Dr. Olaf Fuhr, and Prof. Dieter Fenske for their assistance in PXRD and SC-XRD measurements, and Dr. Papri Chakraborty for the ESI-MS measurements.

■ REFERENCES

(1) Moessner, R.; Ramirez, A. P. Geometrical Frustration. *Phys. Today* **2006**, *59*, 24−29.

(2) Schnack, J. Effects of Frustration on Magnetic Molecules: A Survey from Olivier Kahn until Today. *Dalton Trans.* **2010**, *39* (20), 4677.

(3) Harrison, A. First Catch Your Hare: The Design and Synthesis of Frustrated Magnets. *J. Phys.: Condens. Matter* **2004**, *16* (11), S553−S572.

(4) Chen, H.; Manvell, A. S.; Kubus, M.; Dunstan, M. A.; Lorusso, G.; Gracia, D.; Jørgensen, M. S. B.; Kegnæs, S.; Wilhelm, F.; Rogalev, A.; Evangelisti, M.; Pedersen, K. S. Towards Frustration in Eu(Ii) Archimedean Tessellations. *Chem. Commun.* **2023**, *59* (12), 1609−1612.

(5) Lorusso, G.; Sharples, J. W.; Palacios, E.; Roubeau, O.; Brechin, E. K.; Sessoli, R.; Rossin, A.; Tuna, F.; McInnes, E. J. L.; Collison, D.; Evangelisti, M. A Dense Metal-Organic Framework for Enhanced Magnetic Refrigeration. *Adv. Mater.* **2013**, *25* (33), 4653−4656.

(6) Sharples, J. W.; Collison, D.; McInnes, E. J. L.; Schnack, J.; Palacios, E.; Evangelisti, M. Quantum Signatures of a Molecular Nanomagnet in Direct Magnetocaloric Measurements. *Nat. Commun.* **2014**, *5*, 3−8.

(7) Pineda, E. M.; Lorusso, G.; Zangana, K. H.; Palacios, E.; Schnack, J.; Evangelisti, M.; Winpenny, R. E. P.; McInnes, E. J. L. Observation of the Influence of Dipolar and Spin Frustration Effects on the Magnetocaloric Properties of a Trigonal Prismatic {Gd7} Molecular Nanomagnet. *Chem. Sci.* **2016**, *7* (8), 4891−4895.

(8) Moreno Pineda, E.; Heesing, C.; Tuna, F.; Zheng, Y. Z.; McInnes, E. J. L.; Schnack, J.; Winpenny, R. E. P. Copper Lanthanide Phosphonate Cages: Highly Symmetric {Cu3Ln9P6} and {Cu6Ln6P6} Clusters with C 3v and D3h Symmetry. *Inorg. Chem.* **2015**, *54* (13), 6331−6337.

(9) Palacios, M. A.; Moreno Pineda, E.; Sanz, S.; Inglis, R.; Pitak, M. B.; Coles, S. J.; Evangelisti, M.; Nojiri, H.; Heesing, C.; Brechin, E. K.; Schnack, J.; Winpenny, R. E. P. Copper Keplerates: High-Symmetry Magnetic Molecules. *ChemPhysChem* **2016**, *17* (1), 55−60.

(10) Schmidt, R.; Richter, J.; Schnack, J. Frustration Effects in Magnetic Molecules. *J. Magn. Magn. Mater.* **2005**, *295* (2), 164−167.

(11) Sessoli, R. Chilling with Magnetic Molecules. *Angew. Chem., Int. Ed.* **2012**, *51* (1), 43−45.

(12) Evangelisti, M.; Brechin, E. K. Recipes for Enhanced Molecular Cooling. *Dalton Trans.* **2010**, *39* (20), 4672.

(13) Zheng, Y. Z.; Zhou, G. J.; Zheng, Z.; Winpenny, R. E. P. Molecule-Based Magnetic Coolers. *Chem. Soc. Rev.* **2014**, *43* (5), 1462−1475.

(14) Zheng, Y. Z.; Evangelisti, M.; Winpenny, R. E. P. Co-Gd Phosphonate Complexes as Magnetic Refrigerants. *Chem. Sci.* **2011**, *2* (1), 99−102.

(15) Zheng, Y. Z.; Evangelisti, M.; Winpenny, R. E. P. Large Magnetocaloric Effect in a Wells-Dawson Type {Ni6Gd 6P6} Cage. *Angew. Chem., Int. Ed.* **2011**, *50* (16), 3692−3695.

(16) Pineda, E. M.; Tuna, F.; Zheng, Y. Z.; Teat, S. J.; Winpenny, R. E. P.; Schnack, J.; McInnes, E. J. L. Iron Lanthanide Phosphonate

Clusters: {Fe6Ln6P 6} Wells-Dawson-like Structures with D3d Symmetry. *Inorg. Chem.* **2014**, *53* (6), 3032−3038.
(17) Tziotzi, T. G.; Gracia, D.; Dalgarno, S. J.; Schnack, J.; Evangelisti, M.; Brechin, E. K.; Milios, C. J. A $\{Gd_{12}Na_6\}$ Molecular Quadruple-Wheel with a Record Magnetocaloric Effect at Low Magnetic Fields and Temperatures. *J. Am. Chem. Soc.* **2023**, *145* (14), 7743−7747.
(18) Lorusso, G.; Roubeau, O.; Evangelisti, M. Rotating Magnetocaloric Effect in an Anisotropic Molecular Dimer. *Angew. Chem., Int. Ed.* **2016**, *55* (10), 3360−3363.
(19) Konieczny, P.; Czernia, D.; Kajiwara, T. Rotating Magnetocaloric Effect in Highly Anisotropic TbIII and DyIII Single Molecular Magnets. *Sci. Rep.* **2022**, *12* (1), 16601.
(20) Zhitomirsky, M. E.; Honecker, A. Magnetocaloric Effect in One-Dimensional Antiferromagnets. *J. Stat. Mech.: Theory Exp.* **2004**, *2004* (07), P07012.
(21) Honecker, A.; Wessel, S. Magnetocaloric Effect in Two-Dimensional Spin-1/2 Antiferromagnets. *Phys. B: Condens. Matter* **2006**, *378*−*380* (SPEC), 1098−1099.
(22) Derzhko, O.; Richter, J. Finite Low-Temperature Entropy of Some Strongly Frustrated Quantum Spin Lattices in the Vicinity of the Saturation Field. *Phys. Rev. B* **2004**, *70* (10), 104415.
(23) Alvarez, S.; Alemany, P.; Casanova, D.; Cirera, J.; Llunell, M.; Avnir, D. Shape Maps and Polyhedral Interconversion Paths in Transition Metal Chemistry. *Coord. Chem. Rev.* **2005**, *249*, 1693−1708.
(24) Gagné, O. C.; Hawthorne, F. C. Comprehensive Derivation of Bond-Valence Parameters for Ion Pairs Involving Oxygen. *Acta Crystallogr., Sect. B: Struct. Sci., Cryst. Eng. Mater.* **2015**, *71*, 562−578.
(25) Jaklič, J.; Prelovšek, P. Lanczos Method for the Calculation of Finite-Temperature Quantities in Correlated Systems. *Phys. Rev. B* **1994**, *49* (7), 5065−5068.
(26) Schnack, J.; Richter, J.; Steinigeweg, R. Accuracy of the Finite-Temperature Lanczos Method Compared to Simple Typicality-Based Estimates. *Phys. Rev. Res.* **2020**, *2* (1), 013186.

https://doi.org/10.1021/jacs.5c13048
J. Am. Chem. Soc. XXXX, XXX, XXX−XXX